Earth and Planetary Science Letters ••• (••••) •••–•••

Contents lists available at ScienceDirect

Earth and Planetary Science Letters

www.elsevier.com/locate/epsl

Iridium profiles and delivery across the Cretaceous/Paleogene boundary

Selen Esmeray-Senlet [a,*,1], Kenneth G. Miller [a], Robert M. Sherrell [a,b], Turgay Senlet [c], Johan Vellekoop [d], Henk Brinkhuis [e]

[a] Department of Earth and Planetary Sciences, Rutgers University, Piscataway, NJ, 08854, USA
[b] Department of Marine and Coastal Sciences, Rutgers University, New Brunswick, NJ, 08901, USA
[c] Google Inc., 3300 N Interstate Hwy 35, Austin, TX, 78705, USA
[d] Division Geology, Department of Earth and Environmental Sciences, KU Leuven University, Celestijnenlaan 200E, 3001, Leuven, Belgium
[e] Marine Palynology & Paleoceanography, Department of Earth Sciences, Faculty of Geosciences, Utrecht University, Laboratory of Palaeobotany and Palynology, Budapestlaan 4, 3584CD, Utrecht, Netherlands

ARTICLE INFO

Article history:
Received 18 March 2016
Received in revised form 4 October 2016
Accepted 7 October 2016
Available online xxxx
Editor: H. Stoll

Keywords:
K/Pg boundary
impact iridium
iridium inventory
advection–diffusion model
bioturbation

ABSTRACT

We examined iridium (Ir) anomalies at the Cretaceous/Paleogene (K/Pg) boundary in siliciclastic shallow marine cores of the New Jersey Coastal Plain, USA, that were deposited at an intermediate distance (~2500 km) from the Chicxulub, Mexico crater. Although closely spaced and generally biostratigraphically complete, the cores show heterogeneity in terms of preservation of the ejecta layers, maximum concentration of Ir measured (~0.1–2.4 ppb), and total thickness of the Ir-enriched interval (11–119 cm). We analyzed the shape of the Ir profiles with a Lagrangian particle-tracking model of sediment mixing. Fits between the mixing model and measured Ir profiles, as well as visible burrows in the cores, show that the shape of the Ir profiles was determined primarily by sediment mixing via bioturbation. In contrast, Tighe Park 1 and Bass River cores show post-depositional remobilization of Ir by geochemical processes. There is a strong inverse relationship between the maximum concentration of Ir measured and the thickness of the sediments over which Ir is spread. We show that the depth-integrated Ir inventory is similar in the majority of the cores, indicating that the total Ir delivery at time of the K/Pg event was spatially homogeneous over this region. Though delivered through a near-instantaneous source, stratospheric dispersal, and settling, our study shows that non-uniform Ir profiles develop due to changes in the regional delivery and post-depositional modification by bioturbation and geochemical processes.

1. Introduction

The discovery of anomalously high abundance of iridium (Ir) and other platinum group elements (PGEs) at the Cretaceous/Paleogene (K/Pg) boundary led to the hypothesis that the Earth was impacted by an ~8–10 km diameter asteroid, causing severe environmental disturbance (Alvarez et al., 1980; Smit and Hertogen, 1980). The impact hypothesis was supported by the subsequent discovery of shocked minerals (Bohor et al., 1987), impact spherules, and Ni-rich spinels (Smit and Kyte, 1984). Discovery of the buried Chicxulub crater, ~180–200 km in diameter in Yucatan Peninsula, Mexico (Hildebrand et al., 1991) also substantiated that the source of Ir and other PGEs is extraterrestrial.

An extraterrestrial source is not the only means of yielding high Ir concentrations at the K/Pg boundary. Deccan flood basalts in modern-day India spanning the K/Pg boundary have been suggested as a source for the Ir anomalies at the boundary (Officer and Drake, 1985). Emplacement of Deccan basalts took ~600 kyr primarily during Chron C29r (Courtillot et al., 1986). Previous studies have suggested that the main pulse began ~340 kyr prior to the K/Pg boundary (Robinson et al., 2009), and ended at the K/Pg boundary (Chenet et al., 2007; Keller et al., 2008), though more recent studies suggest the largest pulse began at about the time of the boundary (Renne et al., 2015) or 250 kyr before the boundary (Schoene et al., 2015). The suggestion that the origin of anomalies in Ir and other platinum group elements (PGEs) are volcanic rather than extraterrestrial has been challenged by mea-

* Corresponding author at: Department of Earth and Planetary Sciences, Rutgers University, Piscataway, NJ, 08854, USA.
E-mail addresses: selenesmeray@gmail.com, selenesmeray@chevron.com (S. Esmeray-Senlet).
[1] Currently at Chevron Energy Technology Company, 1500 Louisiana St., Houston, TX, 77002, USA.

http://dx.doi.org/10.1016/j.epsl.2016.10.010
0012-821X/

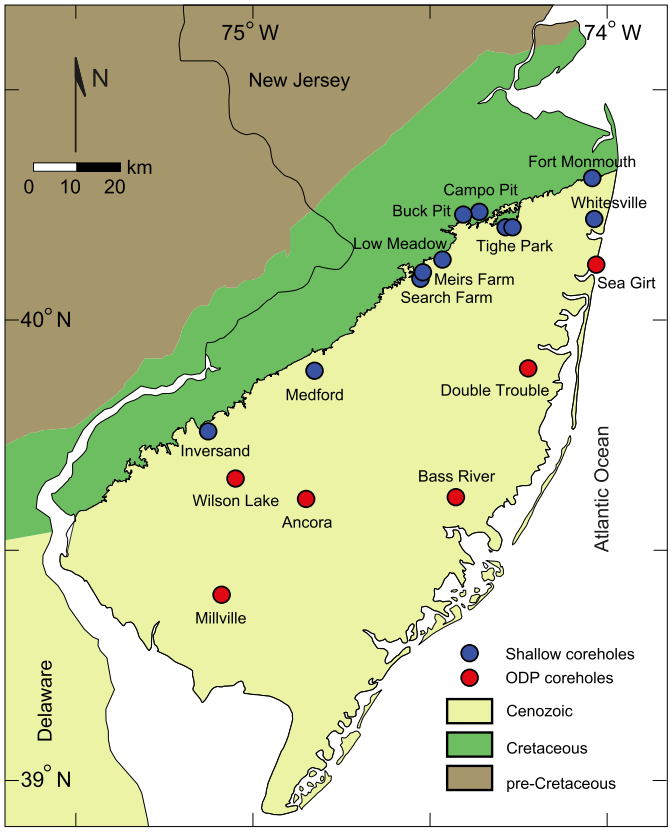

Fig. 1. Geological map of the New Jersey Coastal Plain showing coreholes that sampled the K/Pg boundary. ODP Leg 174AX and ODP Leg 150X cores are shown as red circles. Shallow cores are shown in blue circles. (For interpretation of the references to color in this figure legend, the reader is referred to the web version of this article.)

surements of sedimentary PGE ratios, showing similarity to those of meteorites rather than terrestrial basalts (Evans and Chai, 1997; Evans et al., 1993; Koeberl, 2002). In addition, Sawlowicz (1993) and Shukla et al. (2001) proposed that the contribution of Deccan basalts was too small and local to explain the global inventory of Ir at the K/Pg boundary.

Iridium anomalies, mostly associated with ejecta layers (Smit, 1999; Schulte et al., 2010), have been recorded in more than 85 K/Pg boundary sites globally (Claeys et al., 2002; Schulte et al., 2010). The global occurrence of an Ir anomaly suggests that dust and vapor from the impacting bolide and target rock rich in high-PGE meteoritic material were transported to the stratosphere creating a homogeneous cloud encircling the Earth. Then, Ir-rich material settled down from the atmosphere on scales of months (Toon et al., 1982) and slowly settled through the water column (Claeys et al., 2002).

Outside the Gulf of Mexico, i.e., in the intermediate and distal sites from the Chicxulub crater, there is no correlation between the peak Ir concentration and distance from the impact site (Claeys et al., 2002). The original Ir-rich deposits can be redistributed due to remobilization by sedimentary processes including bioturbation and geochemical remobilization that can account for the site to site differences in Ir concentrations (Sawlowicz, 1993; Claeys et al., 2002), as well as the shape of the Ir anomaly profiles (Hull et al., 2011). In some K/Pg boundary sites the Ir anomaly is concentrated in a thin (~1 cm) interval, whereas at other locations it spreads over as much as several meters of section (Smit, 1999; Claeys et al., 2002). Even geographically close sites show different maximum concentrations of Ir and/or different thicknesses over which the Ir enrichment is spread.

The New Jersey Coastal Plain (NJCP) contains a record of the K/Pg extinction (Olsson, 1960), Ir anomaly, and spherules in both outcrops and in cores (Olsson, 1987; Landman et al., 2007; Miller et al., 2010; Esmeray-Senlet et al., 2015; Vellekoop et al., 2016). Shallow cores (<25 m) drilled adjacent to outcrops of the K/Pg boundary localities (Buck Pit 1, Tighe Park 1, Search Farm 1, Meirs Farm 1, Inversand, and Fort Monmouth 3) and deeper cores drilled onshore by Ocean Drilling Program (ODP) 174AX (Ancora, Double Trouble, and Bass River) provide important constraints on the impact-related features across the K/Pg boundary (Fig. 1). Previously, a 6-cm-thick spherule layer immediately above the K/Pg boundary was reported at Bass River with reworked clay clasts and an Ir peak of 2.4 ppb (Olsson et al., 1997). Landman et al. (2007) reported a ~0.5 ppb Ir anomaly from an outcrop section from Tighe Park, Freehold, NJ below a 20-cm thick bed containing Cretaceous markers. Miller et al. (2010) documented Ir anomalies at Buck Pit 1, Tighe Park 1, Search Farm 1, Meirs Farm 1, and Bass River to investigate the stratigraphic relationship between the Ir anomalies and the extinction level. Updip sites yield lower Ir anomaly peak concentration (~0.5 ppb) compared to the downdip Bass River site and each core shows a different shape of Ir profile, despite being deposited in close proximity.

We conducted additional Ir measurements in the Ancora, Double Trouble, Inversand, and Fort Monmouth 3 sites (Fig. 1) in order to quantify Ir concentrations and investigate potential Ir mobility in the New Jersey sections. Here we address two main questions combining new data with the previous results. First, how did vertical redistribution of Ir by sedimentary processes like bioturbation or geochemical remobilization affect the shape of Ir profiles in the NJCP cores, deposited in shallow marine settings at intermediate distances (~2500 km) from the Chicxulub crater? Second, could the variations in peak Ir anomaly concentrations in NJCP cores, ranging from low to moderate, be attributed to bioturbation, geochemical remobilization, redeposition, or simply concentrations of background values? We analyze the shape of Ir profiles by modeling Ir anomalies under a range of mixing conditions with a Lagrangian advection–diffusion sediment mixing model (Hull et al., 2011) and compare the mixing model parameters with physical observations in the cores. In order to place these Ir profiles in a biostratigraphic context, we combine published planktonic foraminiferal and organic-walled dinoflagellate data with additional palynological analyses on Tighe Park 1, Buck Pit 1, and Inversand. Finally, we evaluate the similarities and differences in depth-integrated anomalies (total vertical accumulation) among the NJCP cores, and discuss the relevance of this quantity relative to the more-frequently-used peak Ir concentrations.

2. Analytical techniques

Concentrations of Ir were measured using Sector Field Inductively Coupled Plasma Mass Spectrometry at the Institute of Marine and Coastal Sciences, Rutgers University. Pre-concentration and isolation of Ir from the sediment samples were carried out using a NiS fire-assay technique modified after Ravizza and Pyle (1997). In this method, sediment samples were dried at 105 °C overnight, and ~1 g subsample was finely ground and homogenized using an acid-cleaned agate mortar and pestle. The resulting powder was then mixed with pure Ni powder and sublimed sulfur (2:1 mass ratio), borax (2:1 ratio to sediment mass), and a ^{191}Ir enriched isotope spike prepared in 6.2N HCl and calibrated against an independent NIST-traceable certified ICP-MS primary Ir standard solution (High-Purity Standards). This mixture is then heated to 1000 °C in a muffle furnace for 75 min to allow fusion. After fusion and rapid cooling, the glassy sample was broken to release a bead of NiS containing scavenged Ir. Beads are then dissolved in 6.2N HCl at 190–200 °C on a hot plate until H_2S evolution stops, then

Table 1
Table showing the maximum and minimum concentration of Ir measured in each core, the total thickness of the Ir-enriched interval, average background values, and the integrated Ir signal calculated. Uncertainties for the maximum and minimum values are defined as explained in the text, and uncertainties for the average background values represent the standard deviation of background samples. These background concentrations were calculated for each core individually, by taking the average of the relatively constant values measured above and below the anomalies, excluding the data points of anomalously high Ir concentrations.

Core	Maximum concentration of Ir-measured (ppb)	Minimum concentration of Ir-measured (ppb)	Thickness of the Ir-enriched interval (cm)	Background value (ppb)	Integrated Ir signal (ppb·m)
Ancora	0.130 ± 0.007	0.050 ± 0.005	79.25	0.045 ± 0.003	0.056
Double Trouble	0.157 ± 0.008	0.040 ± 0.004	70.10	0.044 ± 0.003	0.065
Buck Pit 1	0.432 ± 0.022	0.090 ± 0.009	33.53	0.112 ± 0.027	0.064
Tighe Park 1	0.460 ± 0.023	0.060 ± 0.006	30.24	0.118 ± 0.048	0.060
Bass River	2.370 ± 0.119	0.040 ± 0.004	11.00	0.111 ± 0.049	0.062
Search Farm 1	0.401 ± 0.020	0.020 ± 0.002	13.72	0.071 ± 0.042	0.019
Meirs Farm 1	0.494 ± 0.025	0.040 ± 0.004	10.67	0.103 ± 0.030	0.021
Inversand	0.273 ± 0.014	0.030 ± 0.002	28.96	0.038 ± 0.008	0.025

are filtered through cellulose 0.45 µm filters (Millipore HATF) to remove small insoluble particles containing much of the Ir. Filters are then digested in concentrated HNO_3 in 15 mL screw-cap Teflon vial (Savillex). Quantification of Ir concentrations used the method of isotope dilution, which provides accurate concentrations even if Ir recovery is low or variable. Low procedural blanks (equivalent to 7 pg/g) combined with high sensitivity mass spectrometry provide a detection limit of ~10 pg/g = 0.01 ppb. This method yields excellent procedural reproducibility (precision based on analysis of replicate solid subsamples ±5%, 2σ; Table 1) for even the lowest Ir concentrations (40–100 pg/g) found in background samples, allowing unambiguous determination of Ir anomalies. For the lowest background concentrations determined, we conservatively estimate uncertainty at ±10% (2σ; Table 1) because of the magnitude of the procedural blank relative to the sample measurement, and propagated uncertainty in both.

For the foraminiferal and echinoid fecal pellet analyses core samples (20 g) were disaggregated using Calgon solution (5.5 g of sodium metaphosphate per 4 L of water) and washed with tap water through a 63 µm sieve. After drying in an oven at 40 °C, samples were sieved through 250, 150, 125, and 63 µm sieves and each size fraction examined separately with a reflected-light microscope. Echinoid fecal pellets were counted from the 63–250 µm size fraction using a micro-splitter, and number of fecal pellets per gram of sample was determined.

For palynological analysis ~10 g of sample was crushed and oven dried at 60 °C. Samples were then treated with 10% HCl to remove carbonate components and 40% HF to dissolve the siliceous components. The residue was sieved over nylon mesh sieves of 250 µm and 15 µm. From the residue of the 15–250 µm fraction, quantitative slides are prepared on well-mixed, representative fractions. All slides are stored in the collection of the Division Geology, Department of Earth and Environmental Sciences, KU Leuven, Belgium.

3. Vertical sediment mixing and mixing model

Bioturbation is the mixing of the upper part of the sediment column by burrowing of benthic macrofauna, recycling the nutrients in the sediment mixed layer (Jumars et al., 1990). The rate and extent of bioturbation have been investigated quantitatively using geologically instantaneous markers like impact ejecta and volcanic ashes (Glass, 1969; Ruddiman and Glover, 1972; Guinasso and Schink, 1975). Several techniques for modeling the movement of sediment particles across the sediment–water interface and into the permanent sedimentary record have been developed, as reviewed by Meysman et al. (2003). Traditional sediment mixing models are advection–diffusion models, where the record of a sedimentary event is distributed within a mixed layer characterized by a mixing coefficient (which can be modeled identically to a diffusion coefficient) and advected by burrows into layers of sediments that are older than the event (Guinasso and Schink, 1975).

Hull et al. (2011) modified the one-dimensional Lagrangian particle-tracking model with depth-dependent eddy diffusivity of Tanaka and Franks (2008) to model Ir anomaly shapes across the K/Pg boundary. They used the mixing model to explain the observed Ir anomaly shape at North Pacific DSDP Site 577B, Shatsky Rise (their Fig. 5). The model fit the measured Ir profile at Hole 577B, showing a peak concentration of 5.6 ppb in an Ir anomaly that is spread over a ~30-cm-thick bioturbated interval, with an r^2 of 0.95 (Hull et al., 2011). The authors showed that the one-dimensional Lagrangian particle-tracking model is successful in explaining Ir profile shapes, invoking only physical sediment mixing. In this study, we use the mixing model of Hull et al. (2011) to determine whether the anomaly profiles in this shallow water paleo-environment can be similarly explained by bioturbation, and if so what mixing parameters best fit measured iridium anomalies in the NJCP cores.

In the one-dimensional Lagrangian particle-tracking model of Hull et al. (2011), the material is moved based on depth-dependent diffusivity with a non-deterministic approach (Fig. 2). In the model, vertical diffusivity (K_v) is modeled as a decreasing hyperbolic tangent (tanh) function that generates a vertical diffusivity profile that is continuously differentiable with depth (Ross and Sharples, 2004). Vertical diffusivity decreases with depth, causing a well-mixed layer at the top underlain by increasingly poorly mixed sediments. K_v decreases with depth according to:

$$K_v(z) = \frac{K_0}{2}\left[1 - \tanh\left(\frac{z - z_0}{z_{scale}}\right)\right]$$

where z_0 is the depth of the inflection point in the tanh profile, delineating the bottom of the well-mixed layer of sediment; z_{scale} is the e-folding scale for the tanh profile, determining the depth over which mixing asymptotes to zero; and K_0 is the maximum vertical diffusivity defining the upper limit of mixing in the tanh profile (not diffusivity at the sediment–water interface) (Fig. 2).

Modeled iridium is moved vertically by vertical diffusivity as a Markov process, where the depth $z_{t+\Delta t}$ of a particle at time $t + \Delta t$ is a function of the depth (z_t) in the previous time step (t):

$$z_{t+\Delta t} = z_t + \frac{\partial K_v(z_t)}{\partial z}\Delta t + R\left[\frac{2K_v(z_t + \frac{1}{2}\frac{\partial Kv}{\partial z}\Delta t)\Delta t}{r}\right]^{1/2} + w_s\Delta t$$

where R is a random process with a zero mean and a variance of r, where $r = 1/3$. R is selected from a uniform distribution ranging from -1 to 1. Sedimentation rate (w_s) causes the sinking of

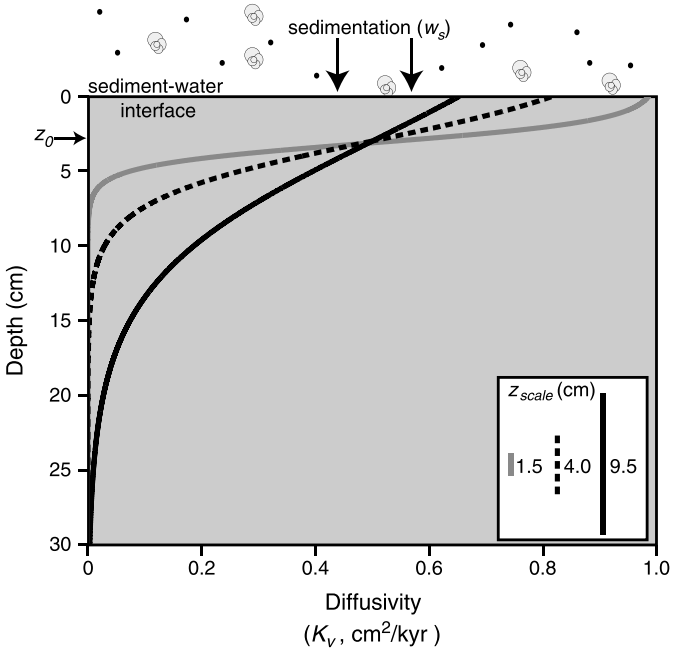

Fig. 2. The Lagrangian sediment mixing model (Hull et al., 2011). Three mixing curves highlight the effect of z_{scale} on depth-dependent diffusivity (K_v). All curves are parameterized with the same z_0, indicated on the depth axis, and the same K_0. Larger values for z_{scale} (black lines) increase the depth range over which K_v asymptotes to zero relative to smaller z_{scale} values (dotted black and gray lines) (Hull et al., 2011, their Fig. 1).

sediment out of the mixed layer continuously. We took the time step Δt as 0.2 yr to account for the low sedimentation rates in the NJCP cores.

We simulated Ir deposition by the introduction of particles into the model at the sediment–water interface, with each particle representing an equal amount of Ir (Hull et al., 2011). At the time of the event (K/Pg boundary), 100,000 particles were injected into the model and mixed according to the different model parameterization. Particle counts were summed with 2 cm deep increments (di) to obtain Ir concentrations.

Earliest Paleocene sedimentation rates were calculated using planktonic foraminiferal and/or dinocysts first and last appearances calibrated to the GTS2012 time scale (Gradstein et al., 2012). Sedimentation rates calculated in the early Danian are 0.2 cm/kyr at Bass River, Ancora, and Inversand and 0.3 cm/kyr at Meirs Farm 1 and Double Trouble. For Search Farm 1, and Tighe Park 1, we do not have enough biostratigraphic information to calculate the sedimentation rates. Therefore, while running the model we tried a combination of possible w_s values (0.1, 0.2, 0.3, 0.4, and 0.5 cm/kyr) with a range of mixing parameters for each core. For all cores best model fit was obtained with sedimentation rates of 0.2–0.3 cm/kyr. These slow sedimentation rates are a product of low Maastrichtian to Danian terrigenous influx (Browning et al., 2008) and a collapse of export pelagic productivity in the region in the Danian (D'Hondt, 2005; Esmeray-Senlet et al., 2015). While food supply was limited in the early Danian on the NJCP (Esmeray-Senlet et al., 2015), heavy bioturbation characterizes the boundary (e.g., Fig. 3 showing the K/Pg boundary at Inversand, NJ).

The combination of mixing parameters K_0 (0.75, 1, 1.5, 5, 10, 100, 250, 1000 cm^2/kyr), z_0 (2, 5, 10, 20, 50, 100, 150 cm), and z_{scale} (1.5, 4, 9.5 cm) were simulated over a period of 1500 yr using MATLAB to get the best fit for the measured Ir profiles. For each model the coefficient of determination (r^2) was calculated to determine how well the model fits the measured Ir profiles. Five models with the highest r^2 are shown in supplementary figures (Figs. S1, S2). The best combination of parameters was selected and model

Fig. 3. Bioturbation at the K/Pg boundary in Inversand outcrop, New Jersey.

simulations were repeated 50 times to take the average, as individual model runs can vary due to the non-deterministic nature of the approach.

Ir concentrations measured in the NJCP cores are much lower than those of European (e.g., Stevns Klint, Denmark; Premovic et al., 2012) and Tunisian (e.g., El Kef, Tunisia; Ben Abdelkader et al., 1997) neritic sections. Although the model of Hull et al. (2011) does not take background levels into account, we consider the background level of each core, since cores with low to moderate Ir anomalies yield low signal to noise ratios. For each core, to find the background level we took the average of the relatively constant values measured above and below the anomalies ($n = 2$ to 16 samples per core) excluding the data points of anomalously high Ir concentrations. The background levels vary between 0.04 ppb to 0.12 ppb (Table 1). In the r^2 calculation we excluded data points less than or equal to the background level. We matched the lowest value of the model to the calculated background level.

4. Stratigraphy and Ir anomalies

The NJCP cores were deposited in shallow shelf settings with paleowater depths of 20 ± 5 to 110 ± 20 m during the Late Cretaceous–Early Paleogene transition (Esmeray-Senlet et al., 2015). Ancora, Double Trouble, and Bass River are downdip cores with paleowater depths of ~70, 80, 100 m, respectively, allowing planktonic foraminiferal habitats and thus biostratigraphy. All other cores are shallower with no or low preservation of planktonic foraminifera. Fortunately, organic-walled dinoflagellate cysts (dinocysts) are abundantly present in these records and allow confident biostratigraphic age control across the K/Pg boundary interval. In addition to biostratigraphy, we counted echinoid fe-

Please cite this article in press as: Esmeray-Senlet, S., et al. Iridium profiles and delivery across the Cretaceous/Paleogene boundary. Earth Planet. Sci. Lett. (2016), http://dx.doi.org/10.1016/j.epsl.2016.10.010

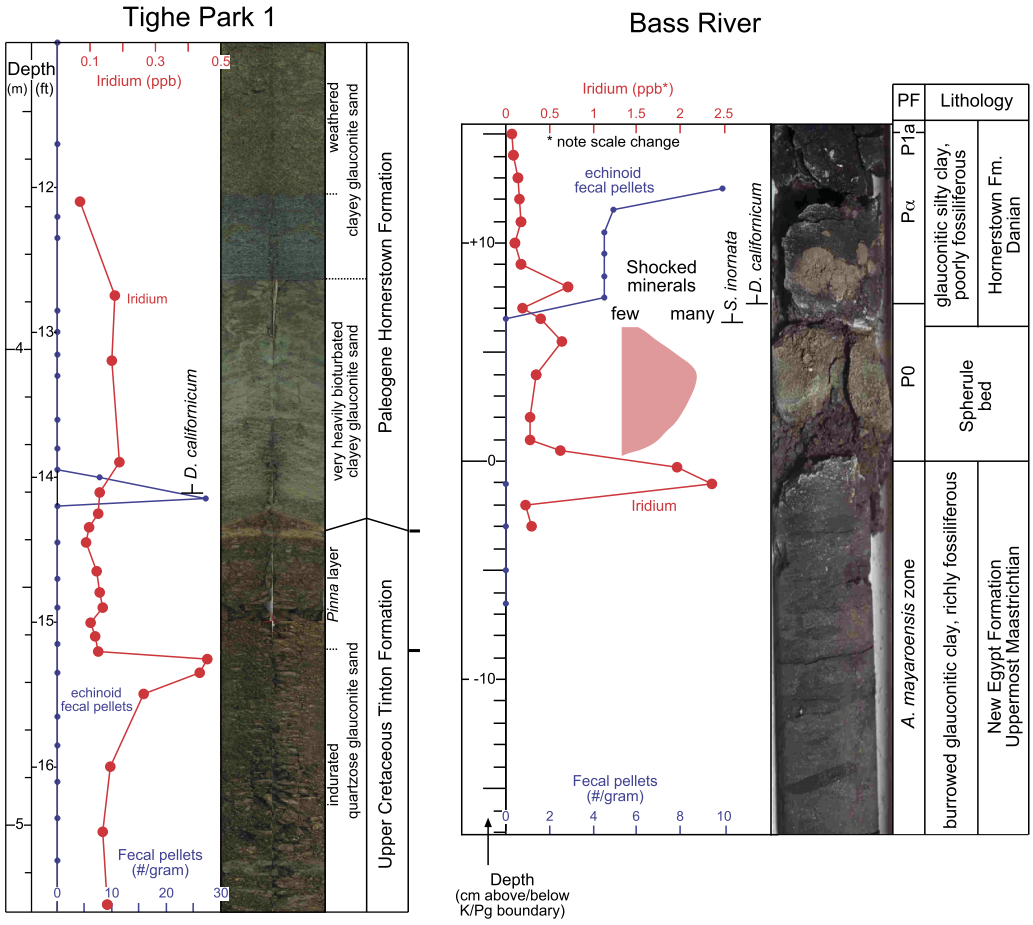

Fig. 4. Ir in parts per billion (ppb), fecal pellets in number/gram of sediment, core photographs, lithology, formational assignments for Tighe Park 1 and Bass River coreholes. Shocked minerals in Bass River are quartz and orthoclase feldspar (see Olsson et al., 1997 for the details of the ejecta layer). Note the lowest occurrences of dinocyst taxa at Tighe Park 1 (after Landman et al., 2007) and Bass River (Olsson et al., 1997). *S.*: *Senoniasphaera*, *D.*: *Damassadinium*. Modified after Miller et al. (2010).

cal pellets that provide a distinct lowermost Danian stratigraphic horizon useful for correlation (Figs. 4–6).

All cores were deposited at a distance ~2500 km from the Chicxulub crater and are considered intermediate sites based on their distance from the impact crater. Intermediate sites are described as having a distance of ~1000 to ~5000 km from the Chicxulub crater with a 2- to 10-cm-thick spherule layer overlain by a 0.2- to 0.5-cm-thick layer having PGE enrichments, shocked minerals, rip-up clasts above the boundary level from tsunamis, and Ni-rich spinels (Smit, 1999; Claeys et al., 2002; Schulte et al., 2010). The NJCP cores show differential preservation of impact related features such as spherule layer, clay clasts, and Ir enrichments (Figs. 4–6).

Bass River, the most complete and downdip core with a paleodepth of ~100 m, shows a biostratigraphically complete upper Maastrichtian to lower Paleogene succession (Fig. 4). The New Egypt Formation was assigned to *Abathomphalus mayaroensis* planktonic foraminifera, *Palynodinium grallator* dinocyst, and *Micula prinsii* nannofossil Zones, representing the uppermost Maastrichtian (Olsson et al., 1997, 2002). Immediately above the Maastrichtian, there is a 6-cm-thick spherule layer with common shocked quartz and feldspar grains and carbonate accretionary lapilli (Olsson et al., 1997, 2002; Yancey and Guillemette, 2008). Sediments above the spherule layer are assigned to Danian planktonic foraminiferal Zones P0 (recognized in one sample, below the first appearance datum of planktonic foraminiferal taxa *Parvularugoglobigerina eugubina*) and *Pα*, recognized by the appearance of *Parvularugoglobigerina eugubina* and the dinoflagellate taxon *Senoniasphaera inornata* (Olsson et al., 1997). A ~3-cm-thick layer of white clay rip-up clasts containing uppermost Cretaceous foraminifera and dinocysts overlies the spherule layer. There is a large Ir anomaly of 2.4 ppb at the base of the spherule bed and two modest Ir anomalies of 0.6 and 0.7 ppb straddling the top of the spherule bed associated with the clast layer.

Ancora (Hole B) is biostratigraphically complete across the K/Pg boundary (Fig. 5), with the presence of planktonic foraminiferal Zones P0 and *Pα* in the earliest Danian (Miller et al., 1999). It contains a 2.6-cm-thick spherule layer with grains of glauconite, intermixed clay, and reworked foraminifera in planktonic foraminiferal Zone P1a (Miller et al., 1999). The presence of glauconite grains and reworked foraminifera in this layer was interpreted as an indication of the redeposition of the original microtektites and a short hiatus between Zones *Pα* and P1a (Miller et al., 1999). There is bioturbation in the 50-cm-thick sediments overlying the boundary. At Ancora there is a low Ir anomaly with a maximum concentration of 0.13 ppb, spread over ~107 cm across the K/Pg boundary.

At Double Trouble, bioturbated clayey glauconite sand of the Upper Cretaceous Navesink Formation is overlain by the very dark green, clayey glauconite sand of the Hornerstown Formation (Fig. 5). A ~3.5 cm-thick calcareous shell layer, assigned to P0/P1a planktonic foraminiferal zone, is present 50 cm above the K/Pg boundary. At Double Trouble, a low Ir anomaly of 0.16 ppb was measured straddling the boundary and covering over ~119 cm.

At Search Farm 1 and Meirs Farm 1, basal Danian glauconite sands of the Hornerstown Formation overlie clayey glauconite sand of the Upper Maastrichtian New Egypt Formation (Fig. 6). The basal Danian is heavily burrowed at Meirs Farm 1, whereas at Search Farm 1, the upper Maastrichtian also shows heavy bioturbation.

Please cite this article in press as: Esmeray-Senlet, S., et al. Iridium profiles and delivery across the Cretaceous/Paleogene boundary. Earth Planet. Sci. Lett. (2016), http://dx.doi.org/10.1016/j.epsl.2016.10.010

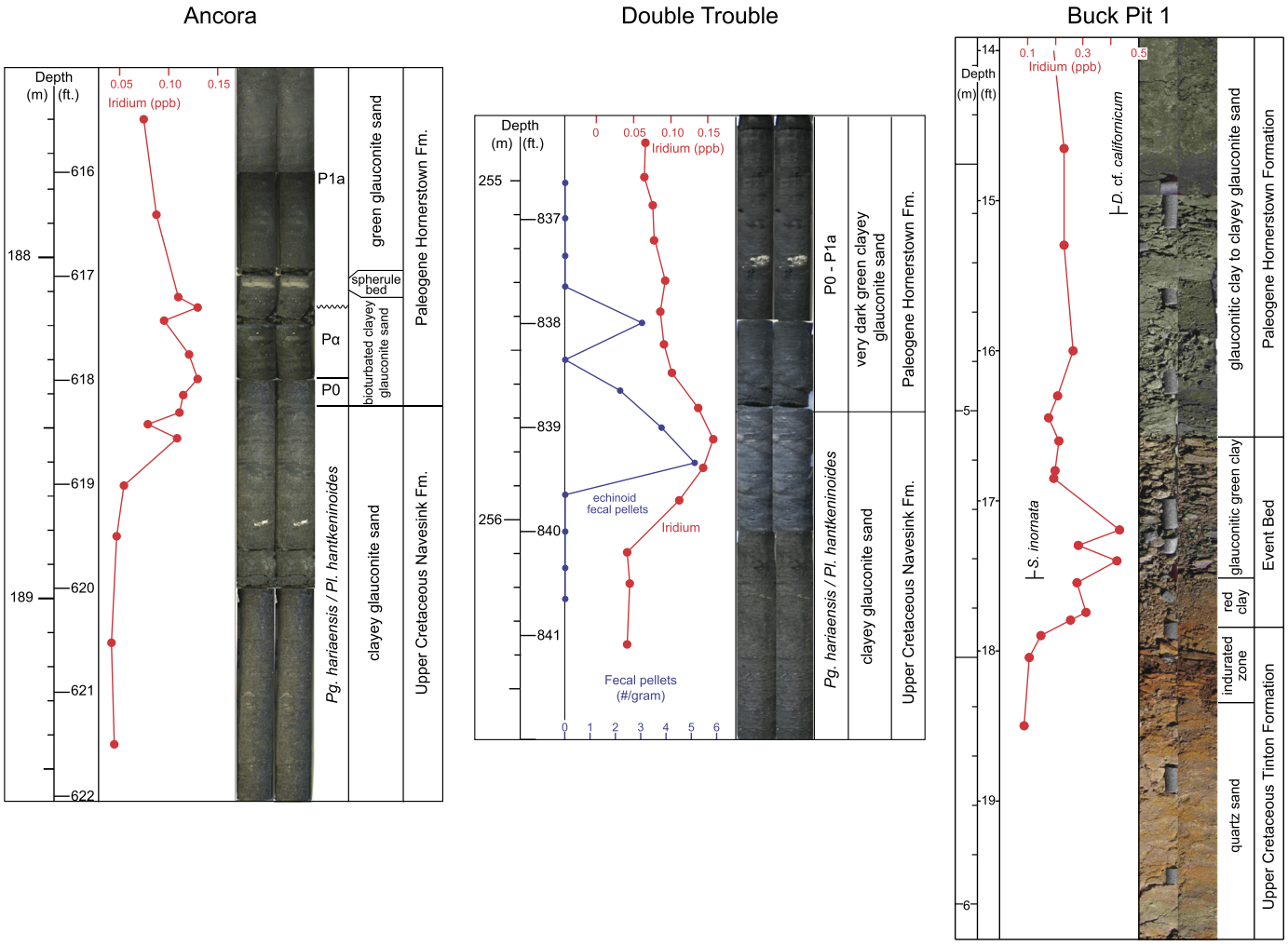

Fig. 5. Ir in parts per billion (ppb), fecal pellets in number/gram of sediment, core photographs, lithology, formational assignments for Ancora, Double Trouble, and Buck Pit 1 coreholes. Planktonic foraminiferal biozones are indicated for Ancora and Double Trouble. Note the lowest occurrences of dinocyst taxa *S. inornata* at adjacent at Buck Pit outcrop (E. Rudolph, 1994 personal commun.) and *D. californicum* at Buck Pit 1(this study). *S.*: *Senoniasphaera*, *D.*: *Damassadinium*. (For interpretation of the references to color in this figure, the reader is referred to the web version of this article.)

Although no distinct spherule layer exists, there is a 5-cm-thick white clay layer at Meirs Farm 1 composed of siderite (Wahyudi, 2010). Although thought to be a clast (Miller et al., 2010) studies of outcrops on adjacent creeks suggest that this is a layer and is likely an alteration of the carbonate spherules and/or carbonate accretionary lapilli (Yancey and Guillemette, 2008). The clay at the K/Pg boundary is associated with a modest Ir anomaly of ~0.5 ppb (Miller et al., 2010) that coincides with an increase in echinoid fecal pellets. At Meirs Farm 1, the lowest occurrence of the lowermost Danian marker taxon *Senoniasphaera* cf. *inornata* (Açıkalın et al., 2015; Vellekoop et al., 2014) occurs at ~5 cm above the white clay layer, followed by a succession of marker taxa such as *Senoniasphaera inornata* s.s. and *Damassadinium* cf. *californicum* (Vellekoop et al., 2016). At Search Farm 1, *Senoniasphaera* cf. *inornata* was not encountered and the lower, but not lowermost, marker taxa *S. inornata* and *D. californicum* occur almost directly above the K-Pg boundary (Vellekoop et al., 2016).

The physical stratigraphy at Buck Pit 1 is slightly different from that in the other cores (Fig. 5). At Buck Pit 1, indurated quartz sand of the uppermost Cretaceous Tinton Formation is overlain by a ~40-cm-thick clay unit. The clay unit consists of a basal red clay and an overlying green clay. The Ir anomaly is spread over the clay unit with a peak of 0.4 ppb in the green clay. Although we did not find any impact spherules at Buck Pit 1 core, the adjacent K/Pg outcrop, Campo Pit, has numerous spherules embedded in clay clasts in the red and green clay (Esmeray-Senlet, 2015) associated with the lowest occurrence of *Senoniasphaera inornata*, a dinocyst marker for the lower Danian (Miller et al., 2010).

At Tighe Park 1, there is 20-cm-thick *Pinna* bed in the uppermost part of the Cretaceous Tinton Formation, directly below the Paleogene Hornerstown Formation, containing a diverse latest Cretaceous fauna including the ammonite *Discoscaphites iris* and the bivalve *Pinna laqueata* in the adjacent outcrop (Landman et al., 2007). Above the *Pinna* bed, the K/Pg boundary is associated with the lowest occurrence of *Damassadinium californicum* and a peak of echinoid fecal pellets (Fig. 4). The Ir anomaly of ~0.5 ppb occurs at the base of the *Pinna* bed, 20 cm below the K/Pg boundary (Miller et al., 2010) confirming the relationship observed between Ir and the *Pinna* bed in the adjacent outcrop in Agony Creek (Landman et al., 2007).

The Inversand Pit at Sewell is known for its well-preserved vertebrate fauna just above the K/Pg boundary. The bone bed in the lowermost Hornerstown Formation, the Main Fossiliferous Layer (MFL), contains the remains of Cretaceous microfossils and macrofossils, including mosasaurs, fish, ammonites, and birds together with Paleogene microfossils (Gallagher, 1993, 2002; Landman et al., 2004, 2007). An Ir concentration of 0.3 ppb occurs in the middle of the 40-cm-thick MFL that is ~50 cm above the Navesink/Horner-

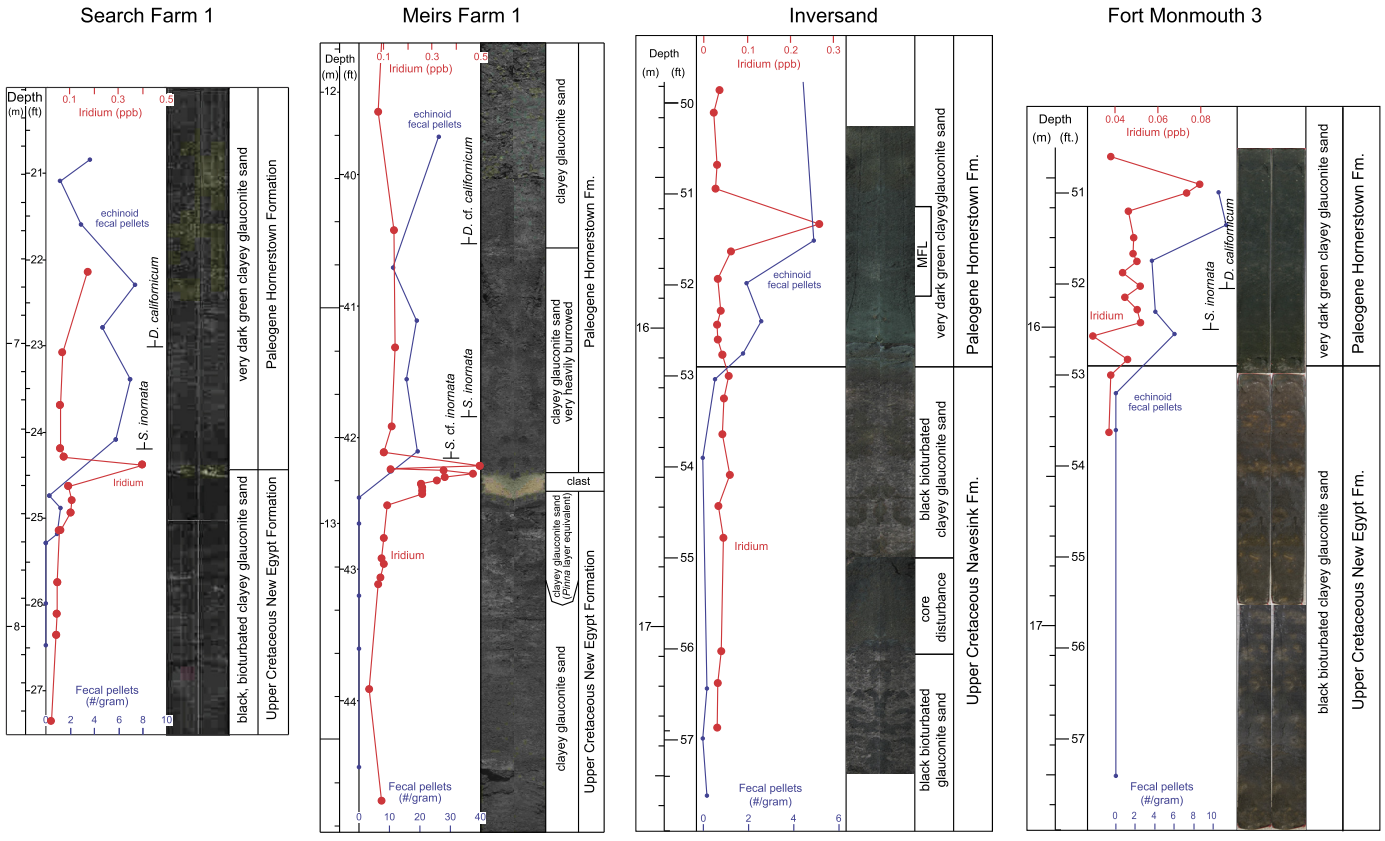

Fig. 6. Ir in parts per billion (ppb), fecal pellets in number/gram of sediment, core photographs, lithology, formational assignments for Search Farm 1, Meirs Farm 1, Inversand, and Fort Monmouth 3 coreholes. Note the lowest occurrences of dinocyst taxa at Search Farm 1, Meirs Farm 1, and Fort Monmouth 3 (Vellekoop et al., 2016). *S.*: *Senoniasphaera*, *D.*: *Damassadinium*.

stown Formation contact (= K/Pg boundary in other cores) (Fig. 6). The absence of an Ir anomaly at the Navesink/Hornerstown formation contact indicates a short hiatus at the K/Pg boundary and reworking of Ir-rich sediments in the MFL that consists of reworked Cretaceous and *in situ* Paleogene fauna.

The stratigraphy of Fort Monmouth 3 is similar to that of adjacent cores, having an increase in echinoid fecal pellets across the lithological contact of New Egypt/Hornerstown Formation contact (Fig. 6). However Ir concentrations across the boundary show only background levels (0.04–0.08 ppb). In the Fort Monmouth 3 core, the lowermost Danian dinocyst marker taxon *Senoniasphaera* cf. *inornata* was not encountered (Vellekoop et al., 2016). In this core, the lowest occurrences of *S. inornata* s.s. and *D. californicum* occur directly at the base of the Hornerstown Fm., suggesting the presence of a short hiatus.

5. Iridium profile shapes

We applied the Lagrangian advection–diffusion mixing model to the NJCP cores, where Ir is scattered across the K/Pg boundary and bioturbation is visible (Ancora, Double Trouble, Buck Pit 1, Search Farm 1, Meirs Farm 1). Mixing model fits to the measured anomaly shapes are very good, with an r^2 of 0.81–0.96.

There is a strong correlation between mixing parameters obtained and physical observations. In the cores in which Ir is dispersed over ~107–119 cm (Double Trouble, Ancora) z_0 (the bottom of the well-mixed layer) is 100–150 cm; cores with Ir dispersion of ~30 cm (Buck Pit 1, Search Farm 1) show z_0 values of 20–50 cm; and cores with Ir dispersion of ~10 cm (Meirs Farm 1) show z_0 values of 20 cm (Figs. 7–8). This indicates that Ir dispersion across the K/Pg boundary can be explained by physical mixing of sediments via bioturbation.

In the Tighe Park 1 and Bass River sections, the Ir peaks do not occur at the same stratigraphic level as the biostratigraphic K/Pg boundary (Fig. 4). Miller et al. (2010) discussed the relative position of the Ir anomaly and mass extinction level in the NJCP cores and concluded that Ir is *in situ*, i.e. at the same level as the biostratigraphic K/Pg boundary, in clay-rich sections, but remobilized geochemically in sandier sections like Tighe Park 1 and Bass River. At Bass River, the highest Ir anomaly occurs 6 cm below the appearance of Danian foraminifera and dinocysts, at the base of the spherule layer as a narrow peak. Because the deposition of Ir takes place slowly as a result of atmospheric fallout it should occur above the ballistic ejecta/spherule layer (Smit, 1999; Kring, 2007). Thus, the Ir enrichment at the base of the spherule layer at Bass River is interpreted as resulting from geochemical remobilization of Ir down section by 6 cm (Miller et al., 2010). Similarly, the Ir anomaly at Tighe Park 1 is a sharp peak at a redox boundary that occurs 20 cm below the appearance of first Danian dinocysts at the base of the porous *Pinna* layer where groundwater percolates from the outcrop (Miller et al., 2010). Both the spherule layer at Bass River and the *Pinna* layer at Tighe Park 1 allowed percolation of Ir that accumulated in a 2- to 3-cm-thick zones as distinct and narrow peaks above these aquicludes (Miller et al., 2010) possibly due to differences in redox potential (Colodner et al., 1992).

At Bass River, a secondary Ir enrichment of ~0.7 ppb straddles the top of the spherule layer, where the original deposition of Ir should have occurred (Fig. 4). Also at Tighe Park 1, ~0.2 ppb Ir is dispersed in the heavily bioturbated clayey glauconite sand of Hornerstown Formation just above the K/Pg boundary (Fig. 4). We applied the mixing model to these intervals, on the assumption that they represent the redistribution of particulate Ir by sediment mixing (Fig. 8). Model mixing parameters obtained for both Bass

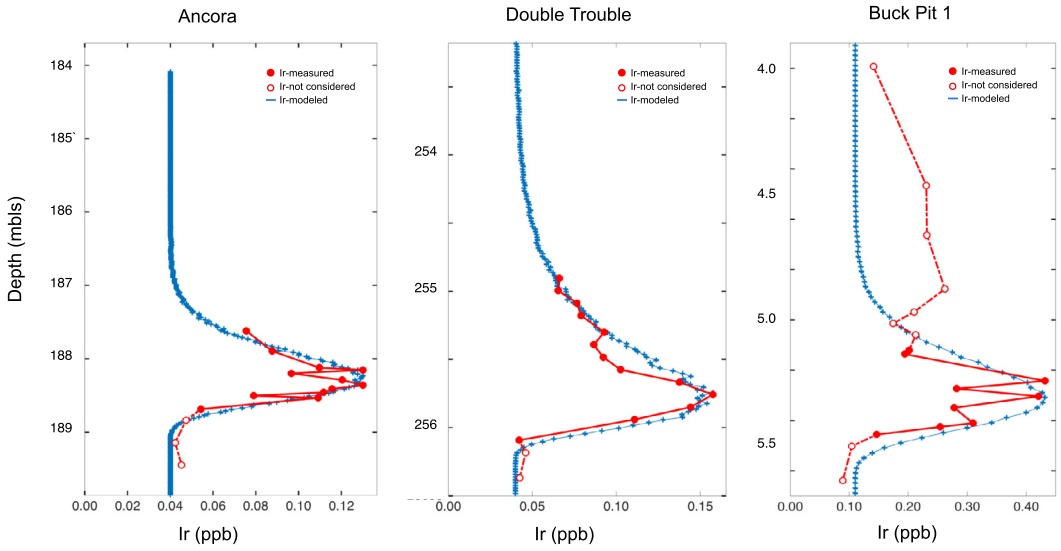

Fig. 7. Modeled Ir profiles for Ancora, Double Trouble, and Buck Pit 1 coreholes that provided best fits to the measured Ir profiles. Ir-modeled is plotted with blue crosses. Ir-measured is plotted with solid red circles; the open red circles show Ir samples that were not considered for the calculation of r^2. The mixing parameters and r^2 values obtained are: Ancora (r^2: 0.88, K_0: 1 cm^2/kyr, z_{scale}: 4 cm, z_0: 150 cm); Double Trouble (r^2: 0.85, K_0: 10 cm^2/kyr, z_{scale}: 9.5 cm, z_0: 100 cm); Buck Pit 1 (r^2: 0.80, K_0: 0.75 cm^2/kyr, z_{scale}: 9.5 cm, z_0: 50 cm). Sedimentation rates (w_s) are 0.2 cm/kyr at Ancora and Buck Pit 1, and 0.3 cm/kyr at Double Trouble. Background values calculated are 0.04 ppb for Ancora and Double Trouble, and 0.11 ppb at Buck Pit 1. mbls: meters below land surface. (For interpretation of the references to color in this figure legend, the reader is referred to the web version of this article.)

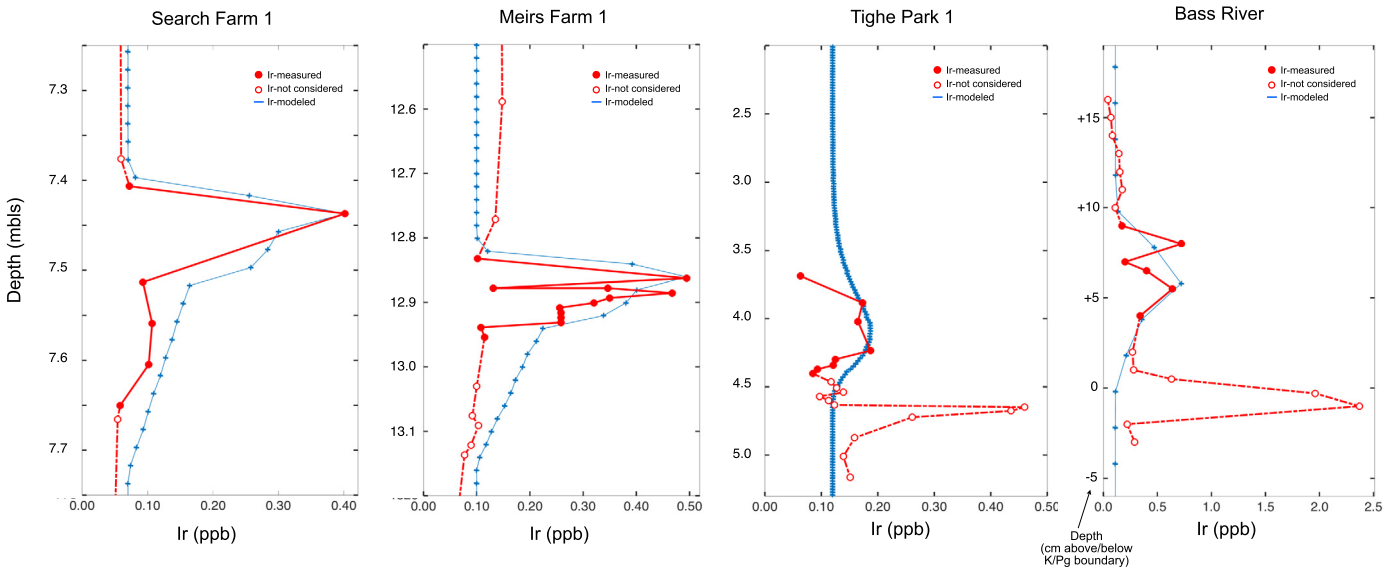

Fig. 8. Modeled Ir profiles for Search Farm 1, Meirs Farm 1, Tighe Park 1, and Bass River coreholes that provided best fits to the measured Ir profiles. Ir-modeled is plotted with blue crosses. Ir-measured is plotted with solid red circles; the open red circles show Ir samples that were not considered for the calculation of r^2. The mixing parameters and r^2 values obtained are: Search Farm 1 (r^2: 0.96, K_0: 1000 cm^2/kyr, z_{scale}: 1.5 cm, z_0: 20 cm); Meirs Farm 1 (r^2: 0.82, K_0: 1000 cm^2/kyr, z_{scale}: 1.5 cm, z_0: 20 cm); Tighe Park 1 (r^2: 0.95, K_0: 10 cm^2/kyr, z_{scale}: 4 cm, z_0: 100 cm); Bass River (r^2: 0.68, K_0: 100 cm^2/kyr, z_{scale}: 1.5 cm, z_0: 10 cm). Sedimentation rates (w_s) are 0.2 cm/kyr at Search Farm 1 and Bass River, and 0.3 cm/yr at Meirs Farm 1 and Tighe Park 1. Background values calculated are 0.07 ppb for Search Farm 1, 0.10 ppb for Meirs Farm 1, 0.11 ppb for Bass River, and 0.12 ppb for Tighe Park 1. mbls: meters below land surface. Note that depth of Bass River is shown in cm above/below the K/Pg boundary. (For interpretation of the references to color in this figure legend, the reader is referred to the web version of this article.)

River and Tighe Park 1 are in line with the physical observations. The best model fit for Tighe Park 1 shows a z_0 of 100 cm, where the dispersion of Ir is ~30 cm; whereas as at Bass River z_0 is 10 cm with an Ir dispersion of ~11 cm.

6. Integrated iridium anomalies and total iridium delivery

The NJCP sites show different Ir profiles across the K/Pg boundary in terms of maximum concentration of Ir measured, total thickness of the Ir-enriched interval, and background values of Ir (Table 1). However, there is a strong inverse relationship between the maximum concentration of Ir measured and the thickness of the Ir diffusion zone. The maximum Ir peak measured is 2.4 ppb at Bass River and the anomaly is concentrated within a 3-cm-thick layer (Fig. 4). Approximately 4 cm above this major peak is a secondary enrichment of ~0.7 ppb that is ~4 cm thick. Including both major and secondary peaks, the total thickness of the Ir enrichment interval at Bass River is 11 cm. Meirs Farm 1, Search Farm 1, Buck Pit 1, and Tighe Park 1 show moderate Ir peaks of ~0.5 ppb that are spread over 10–30 cm (Figs. 5, 6). At Ancora and Double Trouble, where the thickness of the Ir-enriched interval reaches up to ~119 cm, there are much lower maximum concentrations, 0.13

and 0.16 ppb, respectively (Fig. 5). This suggests that Ir was diluted after the original time of deposition due to sedimentary processes of bioturbation and/or geochemical remobilization, causing lower peak Ir anomalies.

We evaluate the integrated Ir signal over the thickness of the Ir-enriched interval using the data above the background levels (Table 1). Using the trapezoidal rule, a technique for approximating the definite integral, we calculated the area of the region that is bounded by the Ir anomalies in each core. The area under the curve, i.e., the integrated Ir signal indicates the total Ir delivery accumulation, independent of the distance over which it was mixed vertically in the core.

Results show that the integrated Ir anomaly at Ancora, Double Trouble, Buck Pit 1, Tighe Park 1, and Bass River are very similar (~0.06 ppb·m), indicating that the total Ir delivery to these cores were comparable (Table 1). Cores having higher Ir maxima, but narrower peak vs. lower Ir maxima and diffused peaks show the same total Ir delivery indicating that the original Ir deposited was spread vertically across the K/Pg boundary by sedimentary and geochemical processes.

Search Farm 1, Meirs Farm 1, and Inversand show similar integrated Ir values to each other, but lower than that of the other cores (~0.02 ppb·m). At Inversand, the Ir-rich horizon is situated in the MFL, 50 cm above the K/Pg boundary, and is interpreted as reworked. Although the Ir peak is associated with the K/Pg boundary at Search Farm 1 and Meirs Farm 1, short hiatuses at the boundary are also possible, causing lower integrated Ir anomalies in these two cores. However, dinocysts studies indicate that at Meirs Farm 1, the dinocyst marker taxon *Senoniasphaera* cf. *inornata* is present (Vellekoop et al., 2016), indicating that it is biostratigraphically complete, in contrast to the Search Farm 1 and Fort Monmouth 3 cores.

White clasts containing Maastrichtian planktonic foraminifera and outer neritic benthic foraminiferal assemblage were interpreted as rip-ups due to a tsunami that eroded the outer continental shelf and upper slope after a slope failure triggered by earthquakes generated by the Chicxulub impact (Norris et al., 2000; Olsson et al., 2002). This tsunami was distinguished from the impact-generated mega-tsunami that reworked sediments in the Gulf of Mexico, since Florida and Bahama platforms prevented tsunamis from spreading from the Gulf of Mexico into the western North Atlantic (Norris et al., 2000). This can also explain the heterogeneity of the preservation of the spherules on the NJCP (Miller et al., 2010).

7. Conclusions

The shape of the Ir profiles across the K/Pg boundary and the maximum Ir concentrations measured are highly variable among shallow shelf cores of NJCP, although they were deposited geographically very close to each other. The shape of the Ir profiles and the concentrations measured seem to appear determined primarily by sedimentary and geochemical processes, especially bioturbation. Evidence supporting sediment mixing are burrows visible in the cores and good fits between mixing model and measured Ir profiles.

Using the Lagrangian advection–diffusion model (Hull et al., 2011), we were able to show the extent of mixing effects on the Ir records quantitatively across the K/Pg boundary at 7 shallow-water cores in the NJCP. Modeling and fitting the model to the measured iridium profiles showed that Ir anomaly shapes could generally be explained by sediment mixing. Hull et al. (2011) showed that the model is successful in explaining Ir profiles in a distal deep-sea site (Site 577B) with a less complicated mixing history. Our modeling effort in shallow water cores at intermediate distance from the impact site showed that the model is also applicable in sites with much more complicated mixing histories. However, the mixing model should be applied carefully taking the background values into account, where there is low signal-to-background ratio with low to moderate Ir concentrations. Furthermore, for complex profiles, the model occasionally fails to fit secondary peaks.

Our evaluation showed that the integrated Ir signal in the majority of cores is indistinguishable in the NJCP, strongly suggesting that the total Ir delivery to this region was uniform at time of K/Pg event. Although having received comparable mass of Ir, the sites show different maximum concentrations of Ir that are inversely proportional to the total thickness of the Ir-enriched interval. Interregional comparison show that variations in Ir accumulations vary regionally and locally despite a near-instantaneous source, stratospheric dispersal, and settling. Non-uniform Ir profiles develop due to changes in the regional delivery and post-depositional modification by bioturbation and migration to redox boundaries. This provides additional evidence of mixing dilution of Ir after the original time of deposition. Additional elemental analysis is suggested as future work in order to supply further evidence of Ir remobilization to redox boundaries.

It has been often thought that low Ir concentrations at the K/Pg boundary shows the incompleteness of the boundary or might only be reflecting the accumulation of cosmic dust due to low sedimentation rates (Sawlowicz, 1993). The findings of this study, however, show that even modest Ir concentrations are a product of a single global cause: the Chicxulub impact.

Acknowledgements

We thank DOSECC (Drilling, Observation and Sampling of the Earths Continental Crust) for partially funding this study through their Research Grants in Scientific Drilling, S. Tuorto and P. Field for helping apply the NiS fire-assay method, J.V. Browning for assistance with the cores, R.K. Olsson for advice on planktonic foraminiferal biostratigraphy, the USGS Eastern Geology and Paleoclimate Center drillers, and comments from two reviewers (C. Koeberl and anonymous). Supported by NSF Grants EAR-070778, OCE-0751757, OCE-1154379, and OCE14-63759 (Miller).

Appendix A. Supplementary material

Supplementary material related to this article can be found online at http://dx.doi.org/10.1016/j.epsl.2016.10.010.

References

Açıkalın, S., Vellekoop, J., Ocakoğlu, F., Yılmaz, İ.Ö., Smit, J., Ozkan Altiner, S., Goderis, S., Vonhof, H., Speijer, R., Voelders, L., Fornaciari, E., Brinkhuis, H., 2015. Geochemical and palaeontological characterization of a new K-Pg boundary locality from the Northern branch of the Neo-Tethys: Mudurnu–Göynük basin, NW Turkey. Cretac. Res. 52, 251–267.

Alvarez, L., Alvarez, W., Asaro, F., Michel, H., 1980. Extraterrestrial cause for the Cretaceous–Tertiary extinction. Science 208, 1095–1108.

Ben Abdelkader, O., Ben Salem, H., Donze, P., Maamouri, A., Méon, H., Robin, É., Rocchia, R., Froget, L., 1997. The K/T stratotype section of El Kef (Tunisia): events and biotic turnovers. Geobios 21, 235–245.

Bohor, B., Modreski, P., Foord, E., 1987. Shocked quartz in the Cretaceous–Tertiary boundary clays: evidence for a global distribution. Science 236, 705–709.

Browning, J.V., Miller, K.G., Sugarman, P.J., Kominz, M.A., McLaughlin Jr., P.P., Kulpecz, A.A., Feigenson, M.D., 2008. 100 Myr record of sequences, sedimentary facies and sea level change from Ocean Drilling Program onshore coreholes, US Mid-Atlantic coastal plain. Basin Res. 20, 227–248. http://dx.doi.org/10.1111/j.1365-2117.2008.00360.x.

Chenet, A., Quidelleur, X., Fluteau, F., Courtillot, V., Bajpai, S., 2007. 40K–40Ar dating of the Main Deccan large igneous province: further evidence of KTB age and short duration. Earth Planet. Sci. Lett. 263, 1–15.

Claeys, P., Kiessling, W., Alvarez, W., 2002. Distribution of Chicxulub ejecta at the Cretaceous–Tertiary boundary. In: Koeberl, C., MacLeod, K.G. (Eds.), Catastrophic Events and Mass Extinctions: Impacts and Beyond. In: Spec. Pap., Geol. Soc. Am., vol. 356, pp. 55–68.

Colodner, D., Boyle, E., Edmond, J., Thomson, J., 1992. Post-depositional mobility of platinum, iridium and rhenium in marine sediments. Nature 358, 402–404.

Courtillot, V., Besse, J., Vandamme, D., 1986. Deccan flood basalts at the Cretaceous/Tertiary boundary? Earth Planet. Sci. Lett. 80, 361–374.

D'Hondt, S., 2005. Consequences of the Cretaceous/Paleogene mass extinction for marine ecosystems. Annu. Rev. Ecol. Evol. Syst. 36, 295–317.

Esmeray-Senlet, S., 2015. Biotic, Paleoceanographic, and Stratigraphic Changes Across the Cretaceous/Paleogene Boundary. Doctoral dissertation. Rutgers University. 235 pp.

Esmeray-Senlet, S., Wright, J.D., Olsson, R.K., Miller, K.G., Browning, J.V., Quan, T.M., 2015. Evidence for reduced export productivity following the Cretaceous/Paleogene mass extinction. Paleoceanography 30. http://dx.doi.org/10.1002/2014PA002724.

Evans, N., Chai, C., 1997. The distribution and geochemistry of platinum-group elements as event markers in the Phanerozoic. Palaeogeogr. Palaeoclimatol. Palaeoecol. 132, 373–390.

Evans, N., Gregoire, D., Grieve, R., Goodfellow, W., Veizer, J., 1993. Use of platinum-group elements for impactor identification: terrestrial impact craters and Cretaceous–Tertiary boundary. Geochim. Cosmochim. Acta 57, 3737–3748.

Gallagher, W.B., 1993. The Cretaceous/Tertiary mass extinction event in the northern Atlantic Coastal Plain. Mosasaur 5, 75–155.

Gallagher, W.B., 2002. Faunal changes across the Cretaceous–Tertiary (K-T) boundary in the Atlantic Coastal Plain of New Jersey: restructuring the marine community after the K-T mass-extinction event. In: Koeberl, C., MacLeod, K.G. (Eds.), Catastrophic Events and Mass Extinctions: Impacts and Beyond. In: Spec. Pap., Geol. Soc. Am., vol. 356, pp. 291–301.

Glass, B.P., 1969. Reworking of deep-sea sediments as indicated by vertical dispersion of Australasian and Ivory Coast microtektite horizons. Earth Planet. Sci. Lett. 6, 409–415.

Gradstein, F.M., Ogg, J.G., Schmitz, M., Ogg, G., 2012. The Geologic Time Scale 2012, vols. 1–2. Elsevier BV. 2-volume set, 1176 pp.

Guinasso, N.L., Schink, D.R., 1975. Quantitative estimates of biological mixing rates in abyssal sediments. J. Geophys. Res. 80, 3032–3043.

Hildebrand, A., Penfield, G., Kring, D., Pilkington, M., Camargo, Z., 1991. Chicxulub crater: a possible Cretaceous/Tertiary boundary impact crater on the Yucatan Peninsula, Mexico. Geology 19, 867–871.

Hull, P.M., Franks, P.J.S., Norris, R.D., 2011. Mechanisms and models of iridium anomaly shape across the Cretaceous–Paleogene boundary. Earth Planet. Sci. Lett. 301, 98–106. http://dx.doi.org/10.1016/j.epsl.2010.10.031.

Jumars, P.A., Mayer, L.M., Deming, J.W., Baross, J.A., Wheatcroft, R.A., 1990. Deep-sea deposit-feeding strategies suggested by environmental and feeding constraints. Philos. Trans. R. Soc. Lond. Ser. A, Math. Phys. Sci. 331, 85–101.

Keller, G., Adatte, T., Gardin, S., Bartolini, A., Bajpai, S., 2008. Main Deccan volcanism phase ends near the K-T boundary: evidence from the Krishna–Godavari Basin, SE India. Earth Planet. Sci. Lett. 268, 293–311. http://dx.doi.org/10.1016/j.epsl.2008.01.015.

Koeberl, C., 2002. Mineralogical and geochemical aspects of impact craters. Mineral. Mag. 66, 745–768. http://dx.doi.org/10.1180/0026461026650059.

Kring, D., 2007. The Chicxulub impact event and its environmental consequences at the Cretaceous–Tertiary boundary. Palaeogeogr. Palaeoclimatol. Palaeoecol. 255, 4–21.

Landman, N., Johnson, R., Edwards, L., 2004. Cephalopods from the Cretaceous/Tertiary boundary interval on the Atlantic Coastal Plain, with a description of the highest ammonite zones in North America. Part 1. Maryland and North Carolina. Am. Mus. Novit. 3454, 1–64.

Landman, N.H., Johnson, R.O., Garb, M.P., Edwards, L.E., Kyte, F.T., 2007. Cephalopods from the Cretaceous/Tertiary boundary interval on the Atlantic Coastal Plain, with a description of the highest ammonite zones in North America. Part III. Manasquan River Basin, Monmouth County, Jersey. Bull. Am. Mus. Nat. Hist. 303, 1–122. http://dx.doi.org/10.1206/0003-0090(2007)303[1:CFTTBI]2.0.CO;2.

Meysman, F.J., Boudreau, B.P., Middelburg, J.J., 2003. Relations between local, nonlocal, discrete and continuous models of bioturbation. J. Mar. Res. 61, 391–410.

Miller, K.G., Sugarman, P.J., Browning, J.V., Cramer, B.S., Olsson, R.K., de Romero, L., Aubry, M.-P., Pekar, S.F., Georgescu, M.D., Metzger, K.T., Monteverde, D.H., Skinner, E.S., Uptegrove, J., Mullikin, L.G., et al., 1999. Ancora site. In: Miller, K.G., Sugarman, P.J., Browning, J.V. (Eds.), Proc. Ocean Drill. Program, Initial Rep. 174AX (supplement), 1–65.

Miller, K.G., Sherrell, R., Browning, J.V., Field, M., Gallagher, W., Olsson, R.K., Sugarman, P.J., Tuorto, S., Wahyudi, H., 2010. Relationship between mass extinction and iridium across the Cretaceous–Paleogene boundary in New Jersey. Geology 38, 867–870. http://dx.doi.org/10.1130/G31135.1.

Norris, R.D., Firth, J., Blusztajn, J., Ravizza, G., 2000. Mass failure of the North Atlantic margin triggered by the Cretaceous–Paleogene bolide impact. Geology 28, 1119–1122.

Officer, C., Drake, C., 1985. Terminal Cretaceous environmental events. Science 227, 1161–1167.

Olsson, R.K., 1960. Foraminifera of latest Cretaceous and earliest Tertiary age in the New Jersey Coastal Plain. J. Paleontol. 34, 1–58.

Olsson, R.K., 1987. Cretaceous stratigraphy of the Atlantic Coastal Plain, Atlantic Highlands of New Jersey. In: Geological Society of America Centennial Field Guide – Northeastern Section, pp. 87–90.

Olsson, R.K., Miller, K.G., Browning, J.V., Habib, D., Sugarman, P.J., 1997. Ejecta layer at the Cretaceous–Tertiary boundary, Bass River, New Jersey (Ocean Drilling Program Leg 174AX). Geology 25, 759–762.

Olsson, R.K., Miller, K.G., Browning, J.V., Wright, J.D., Cramer, B.S., 2002. Sequence stratigraphy and sea-level change across the Cretaceous–Tertiary boundary on the New Jersey passive margin. Geol. Soc. (Lond.) Spec. Publ. 356, 97–108.

Premovic, P.I., Ilic, B.S., Djordjevic, M.G., 2012. Iridium anomaly in the Cretaceous–Paleogene boundary at Højerup (Stevns Klint, Denmark) and Woodside Creek (New Zealand): the question of an enormous proportion of extraterrestrial component. J. Serb. Chem. Soc. 77, 247–255. http://dx.doi.org/10.2298/JSC110404178P.

Ravizza, G., Pyle, D., 1997. PGE and Os isotopic analyses of single sample aliquots with NiS fire assay preconcentration. Chem. Geol. 141, 251–268.

Renne, P.R., Sprain, C.J., Richards, M.A., Self, S., Vanderkluysen, L., Kanchan, P., 2015. State shift in Deccan volcanism at the Cretaceous–Paleogene boundary, possibly induced by impact. Science 350, 76–78.

Robinson, N., Ravizza, G., Coccioni, R., Peucker-Ehrenbrink, B., Norris, R.D., 2009. A high-resolution marine Os-187/Os-188 record for the late Maastrichtian: distinguishing the chemical fingerprints of Deccan volcanism and the KP impact event. Earth Planet. Sci. Lett. 281, 159–168. http://dx.doi.org/10.1016/j.epsl.2009.02.019.

Ross, O.N., Sharples, J., 2004. Recipe for 1-D Lagrangian particle tracking models in space-varying diffusivity. Limnol. Oceanogr., Methods 2, 289–302.

Ruddiman, W.F., Glover, L.K., 1972. Vertical mixing of ice-rafted volcanic ash in North Atlantic sediments. Geol. Soc. Am. Bull. 83, 2817–2836.

Sawlowicz, Z., 1993. Iridium and other platinum-group elements as geochemical markers in sedimentary environments. Palaeogeogr. Palaeoclimatol. Palaeoecol. 104, 253–270.

Schoene, B., Samperton, K.M., Eddy, M.P., Keller, G., 2015. U–Pb geochronology of the Deccan Traps and relation to the end-Cretaceous mass extinction. Science 347, 182–184.

Schulte, P., Alegret, L., Arenillas, I., Arz, J.A., Barton, P., Bown, P., Bralower, T.J., Christeson, G., Claeys, P., Cockell, C., 2010. The Chicxulub asteroid impact and mass extinction at the Cretaceous–Paleogene boundary. Science 327, 1214–1218.

Shukla, P., Bhandari, N., Das, A., Shukla, A., Ray, J., 2001. High iridium concentration of alkaline rocks of Deccan and implications to K/T boundary. Proc. Indian Acad. Sci., Earth Planet. Sci. 110, 103–110.

Smit, J., 1999. The global stratigraphy of the Cretaceous–Tertiary boundary impact ejecta. Annu. Rev. Earth Planet. Sci. 27, 75–113.

Smit, J., Hertogen, J., 1980. An extraterrestrial event at the Cretaceous–Tertiary boundary. Nature 285, 198–200.

Smit, J., Kyte, F.T., 1984. Siderophile-rich magnetic spheroids from the Cretaceous–Tertiary boundary in Umbria, Italy. Nature 310, 403–405.

Tanaka, Y., Franks, P.J.S., 2008. Vertical distributions of Japanese Sardine (Sardinops Melanostictus) Eggs: comparison of observations and a wind-forced Lagrangian mixing model. Fish. Oceanogr. 17, 89–100. http://dx.doi.org/10.1111/j.1365-2419.2008.00466.x.

Toon, O.B., Pollack, J.B., Ackerman, T.P., Turco, R.P., McKay, C.P., Liu, M.S., 1982. Evolution of an impact-generated dust cloud and its effects on the atmosphere. Spec. Pap., Geol. Soc. Am. 190, 187–200.

Vellekoop, J., Esmeray-Senlet, S., Miller, K.G., Browning, J.V., Sluijs, A., van de Schootbrugge, B., Sinninghe Damsté, J.S., Brinkhuis, H., 2016. Evidence for Cretaceous–Paleogene boundary bolide "impact winter" conditions from New Jersey, USA. Geology, G37961. http://dx.doi.org/10.1130/G37961.1.

Vellekoop, J., Sluijs, A., Smit, J., Schouten, S., Weijers, J.W.H., Sinninghe Damste, J.S., Brinkhuis, H., 2014. Rapid short-term cooling following the Chicxulub impact at the Cretaceous–Paleogene boundary. Proc. Natl. Acad. Sci. 111, 7537–7541. http://dx.doi.org/10.1073/pnas.1319253111.

Wahyudi, H., 2010. Lithofacies and Depositional Environment Spanning the Cretaceous–Paleogene Boundary on the New Jersey Coastal Plain. M.Sc. thesis. Rutger University, New Brunswick.

Yancey, T.E., Guillemette, R.N., 2008. Carbonate accretionary lapilli in distal deposits of the Chicxulub impact event. Geol. Soc. Am. Bull. 120, 1105–1118.

Please cite this article in press as: Esmeray-Senlet, S., et al. Iridium profiles and delivery across the Cretaceous/Paleogene boundary. Earth Planet. Sci. Lett. (2016), http://dx.doi.org/10.1016/j.epsl.2016.10.010